Directional Heat Dissipation across the Interface in Anatase−Rutile Nanocomposites

Ting Xia,[†] Neng Li,[‡] Yuliang Zhang,[†,§] Michael B. Kruger,[⊥] James Murowchick,[‖] Annabella Selloni,[#] and Xiaobo Chen*,[†]

[†]Department of Chemistry, [⊥]Department of Physics and Astronomy, and [‖]Department of Geosciences, University of Missouri−Kansas City, Kansas City, Missouri 64110, United States

[‡]Center for Photovoltaics and Solar Energy, Shenzhen Institutes of Advanced Technology, Chinese Academy of Sciences, Shenzhen 518055, P. R. China

[§]Institute of Materials Science and Engineering, Shanghai Maritime University, Shanghai 201306, P. R. China

[#]Department of Chemistry, Princeton University, Princeton, New Jersey 08544, United States

Ⓢ *Supporting Information*

ABSTRACT: Understanding the structures and properties of interfaces in (nano-)composites helps to reveal their important influence on reactivity and overall performance. TiO_2 is a technologically important material, and anatase/rutile TiO_2 composites have been shown to display enhanced photocatalytic performance over pure anatase or rutile TiO_2. This has been attributed to a synergistic effect between the two phases, but the origin of this effect as well as the structure of the interface has not been established. Using Raman spectroscopy, here we provide evidence of distinct differences in the thermal properties of the anatase and rutile moieties in the composite, with anatase becoming effectively much warmer than the rutile phase under laser irradiation. With the help of first-principles calculations, we analyze the atomic structure and unique electronic properties of the composite and infer possible reasons for the directional heat dissipation across the interface.

KEYWORDS: anatase/rutile nanocomposite interface, lattice vibrations, Raman spectroscopy, density functional theory, electronic structure
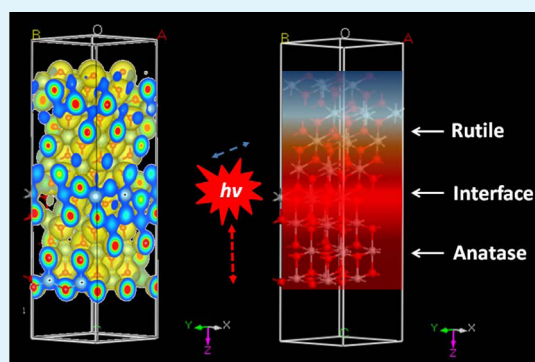
TiO_2 has attracted substantial interest because of its activity for generating hydrogen from water under ultraviolet (UV) light irradiation.[1−5] However, its overall efficiency for solar-driven photocatalysis is very limited, because TiO_2 is a wide band gap semiconductor (3.0 − 3.2 eV) and UV light accounts for less than 5% of the total solar irradiation.[5] Many efforts have been devoted at improving the TiO_2 photocatalytic activity, such as doping with other elements[6−10] and coupling with other phases or compounds.[11−17] In this context, anatase/rutile TiO_2 nanocomposites have been found to display enhanced photocatalytic performance over pure anatase or rutile, due to a synergistic effect between the two phases presumably originating from the interface.[11−17] It was suggested that the interface allows for rapid electron transfer from rutile to anatase,[11,12] the rutile phase acts as an antenna to extend the photoactivity into visible wavelengths, and catalytic "hot spots" exist at the rutile−anatase interface.[11] It was also suggested that within mixed-phase titania there is a morphology of nanoclusters containing atypically small rutile crystallites interwoven with anatase crystallites,[11] but the atomic level details of the resulting interface are incomplete. The difference between the work functions of anatase and rutile in mixed-

phase TiO_2 has been recently proposed to cause the formation of a built-in field, which facilitates the charge transfer across the interface.[14] This solid−solid interface is also regarded as a key structural feature that facilitates charge separation, reduces electron-hole recombination and enhances the photocatalytic efficiency, as well as the locus of defect sites that act as catalytic "hot spots".[17] Recent molecular dynamics (MD) simulations reported that anatase-rutile interfaces are slightly disordered, with the disorder limited to a narrow region at the interface.[18] Moreover, formation of rutile octahedral structures was observed at the anatase side of the interface due to surface rearrangements.[18] Several interfaces between low-index anatase and rutiles surfaces, such as $(110)_r/(101)_a$ or $(100)_r/(100)_a$, were identified as possible stable structures of the mixed-phase catalyst.[18]

Raman spectroscopy has been widely used to characterize crystal phases and to investigate phase transitions in TiO_2.[10,19−22] Anatase TiO_2 is tetragonal with space group I4/

amd, and has 15 optical modes with irreducible representations $1A_{1g} + 1A_{2u} + 2B_{1g} + 1B_{2u} + 3E_g + 2E_u$.[10,20,21] The modes A_{1g}, B_{1g}, and E_g, are Raman active, the modes A_{2u} and E_u are infrared active, and the B_{2u} mode is both Raman and infrared inactive. The Raman active modes E_g (639 cm^{-1}), B_{1g} (519 cm^{-}), and A_{1g} (513 cm^{-1}), are Ti–O bond stretching vibrations, while the modes B_{1g} (399 cm^{-1}), E_g (197 cm^{-1}), and E_g (144 cm^{-1}) are O–Ti–O bending type vibrations.[20] Rutile is tetragonal with space group $P4/mnm$ and has 15 optical modes with the irreducible representation $1A_{1g} + 1A_{2g} + 1A_{2u} + 1B_{1g} + 1B_{2g} + 2B_{1u} + 1E_g + 3E_u$.[19,22] The modes B_{1g}, E_g, A_{1g}, and B_{2g} are Raman active and all consist of motions of anions with respect to stationary central cations, either perpendicular to the c axis (modes B_{1g}, A_{1g}, and B_{2g}), or along the c axis (mode E_g).[22] The size-dependent properties of TiO$_2$ nanocrystals have been investigated with Raman spectroscopy by many groups.[21,23−27] With increasing size of the anatase nanocrystal, the intensity of the E_g mode increases, the frequency shifts, and the linewidth decreases.[21,23−27] Besides the influence of size, stoichiometry defects of titania nanoparticles also affect the broadening of Raman spectra.[27] A recent report demonstrated that Raman peaks originating from the E_g and A_{1g} vibrational modes were related to different crystal planes and provided an approach for measuring the percentage of the exposed facets.[28] Raman studies also suggested that the anatase phase in the surface region can sustain higher calcination temperatures relative to the bulk during the anatase-rutile phase transformation, and the rutile phase starts to form in the inner regions of the agglomerated TiO$_2$ particles.[29] Subsequent studies by the same group showed however that the particle size is the critical parameter determining the anatase-rutile transition temperature, which decreases with the decrease of the initial particle size.[30] Recently, Satoh et al. found evidence of the size dependence of the irreversible anatase-rutile phase transition in TiO$_2$ nanoparticles and proposed a kinetic control nucleation model.[31] Ricci et al. reported a visible light-induced phase transition of TiO$_2$ nanoparticles from anatase to the rutile structure under oxygen-poor conditions, and explained it in the framework of oxygen adsorption and desorption with the involvement of surface oxygen vacancies and F centers.[32] Chatterjee et al. found that carbon inclusions inside or on the surface of TiO$_2$ facilitated the phase transformation from the anatase to the rutile phase at high laser power annealing, by creating oxygen vacancies.[33] Lee et al. performed spontaneous Raman spectroscopy studies on a series of anatase Fe-doped TiO$_2$ nanoparticles and investigated their structural transformation under the exposure of a 532 nm green laser.[34] They found that the anatase phase of TiO$_2$ was effectively converted into the rutile phase with the assistance of Fe doping, and the critical laser intensity for phase transformation decreased with increasing the Fe content, because of the enhanced optical absorption and the photoinduced thermal heating effect associated with the defect structure within the bandgap of Fe-doped TiO$_2$ nanoparticles.[34]

Altogether, the existing literature clearly shows that the structure and properties of the interface play a key role in the structural transformation and photocatalytic performance of anatase/rutile nanocomposites. Understanding these properties is both of scientific and technological interest, as it can help the design of photocatalytic materials with improved performance.[35−37] In this work, we provide fundamental information on three crucial aspects of the interface of anatase/rutile nanocomposites: the atomic structure of the interface from

modeling, the electronic properties from experiment and first-principles calculations, and the unique vibrational and thermal properties of rutile/anatase composites from experimental investigations. These results improve significantly our understanding of the behavior of the TiO$_2$ anatase and rutile polymorphs and highlight the key role of the interface in the properties of the composite.

We prepared the rutile/anatase nanocomposites with the sol−gel method followed by calcination at 550 °C.[16] The crystal structure of the nanocomposites was characterized with X-ray diffraction (PXRD) using a Rigaku Miniflex PXRD machine with Cu Kα as the X-ray sources (wavelength = 1.5418 Å) and the 2θ range was from 15 to 85° with a step width of 0.08 and count time of 3 s/step. The X-ray diffraction pattern shown in Figure 1A suggested the nanocomposites included
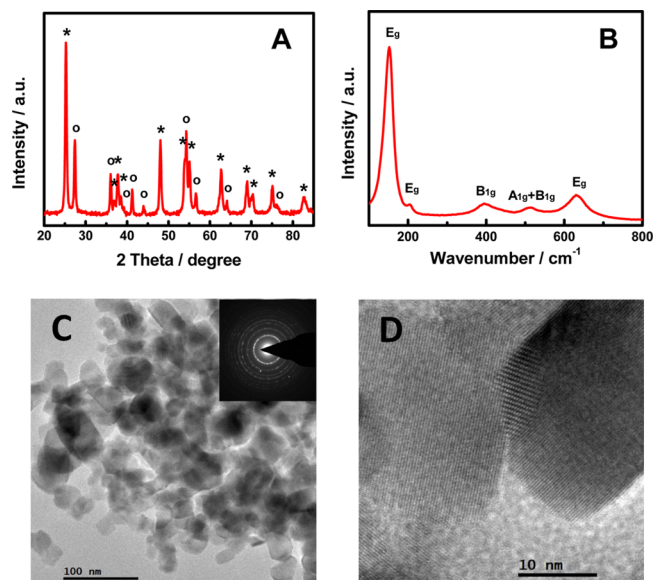
Figure 1. (A) Powder X-ray diffractograms (PXRD) and (B) Raman scattering patterns of anatase/rutile TiO$_2$ nanocomposites (excitation wavelength of 785 nm and laser power of 100 mW). (C) Low-resolution and (D) high-resolution transmission electron microscopy (HRTEM) image. The notations (*) and (o) in (A) point to the anatase and rutile phases, respectively. The inset in C shows a selected area electron diffraction pattern.

both crystalline anatase and rutile phases. The size of the crystalline grain was calculated with the Scherrer equation and the composition was deduced with the Rietveld fittings (see Figure S1 and Table S1 in the Supporting Information). The nanocomposites contained 65% 17 nm anatase and 35% 20 nm rutile. The lattice structure of the nanocomposites was further tested with Raman spectroscopy with the excitation wavelength of 785 nm and laser power of 100 mW. The Raman spectrum of the anatase/rutile nanocomposites in Figure 1B showed however a typical pure anatase scattering pattern with peaks at E_g(a) $\sim$ 146.5 cm^{-1}, E_g(a) $\sim$ 201 cm^{-1}, B_{1g}(a) $\sim$ 399 cm^{-1}, $A_{1g} + B_{1g}$(a) $\sim$ 517 cm^{-1}, and E_g(a) $\sim$ 639 cm^{-1}.[10,20,21] No rutile phase TiO$_2$ was clearly observed. This suggested that in the anatase−rutile nanocomposites, the anatase part was on the outside, whereas the rutile part was in the interior, because the information depth of X-ray diffraction is on the order of tens of micrometers, while Raman scattering tends to provide information sensitive to the surface of the particles. This observation was consistent with a previous study showing that
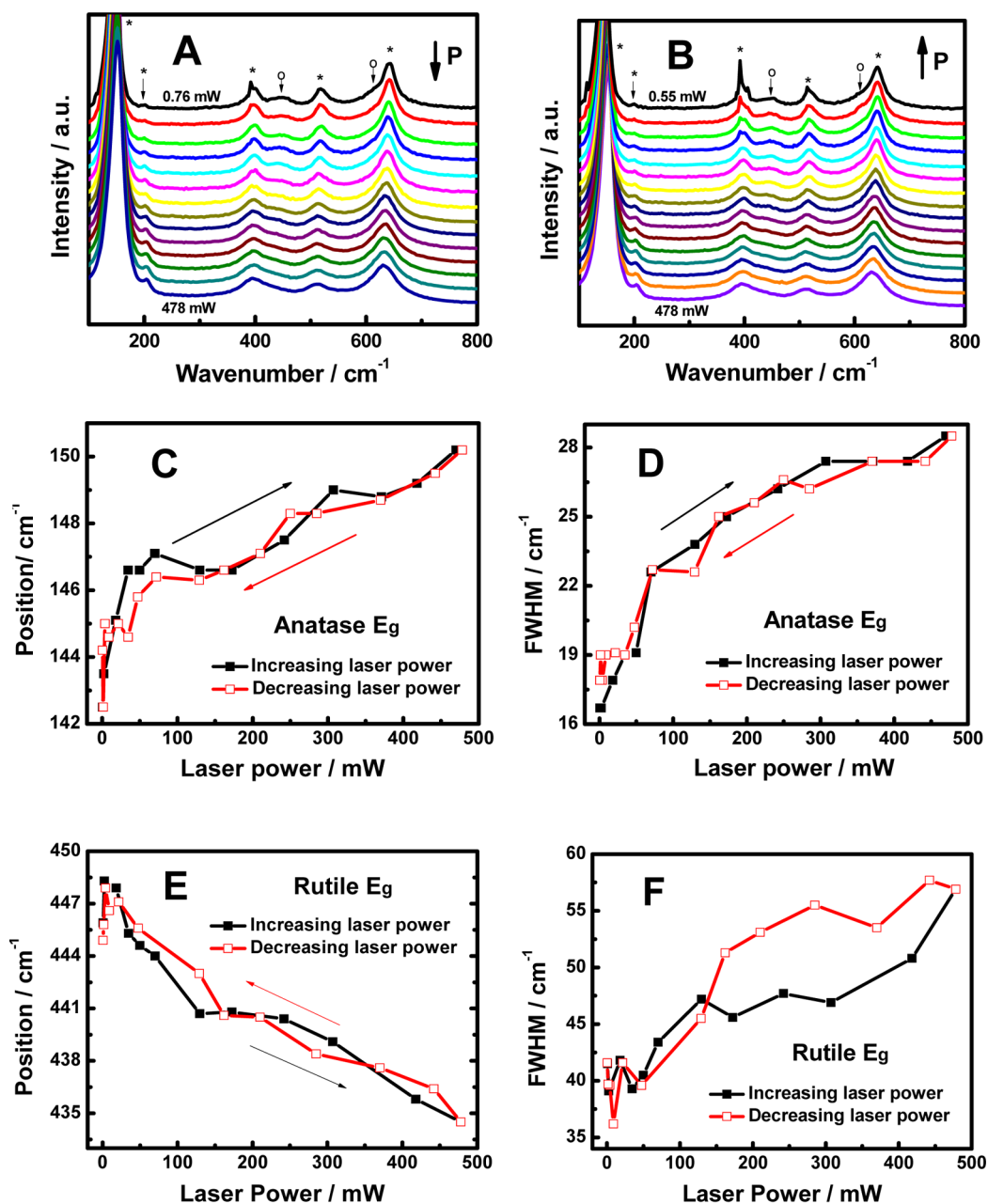
Figure 2. (A) Raman spectrum change of the TiO_2 nanocomposite as LP increased from 0.760 mW to 478.0 mW, (B) Raman spectrum change of the TiO_2 nanocomposite as LP decreased from 478.0 mW to 0.546 mW. All Raman spectra were normalized to the peak near 146 cm^{-1}. The arrows point to the changes of the vibrational modes of anatase and rutile phase. The (*) and (o) denote the peaks from anatase and rutile phases, respectively. The arrows in A and B show the directions of laser power change. (C) Position and (D) FWHM change as a function of LP power for the E_g(a) Raman mode ($\sim$ 146 cm^{-1}) of the anatase phase in the TiO_2 nanocomposite. (E) Position and (F) FWHM change as a function of LP power for the E_g(r) Raman mode ($\sim$ 442 cm^{-1}) of the rutile phase in the TiO_2 nanocomposite.

the rutile phase evolved mainly from the inner regions of the agglomerated TiO_2 particles and the anatase phase in the surface region could sustain higher calcination temperatures relative to the bulk during the anatase–rutile phase transformation induced by heating.[29]

The morphology of the nanocomposites was investigated with transmission electron microscopy (TEM) on a FEI Tecnai F20 TEM with an electron accelerating voltage of 200 kV. The low-resolution TEM image in Figure 1C showed that the anatase/rutile nanocomposites were aggregates made of smaller particles with size in the range from 20 to 50 nm, consistent with the results from XRD measurements. The clear diffraction

pattern in the selected area electron diffraction pattern in the inset of Figure 1C suggested that the anatase–rutile nanocomposites were highly crystallized. The high crystallinity nature of the anatase–rutile nanocomposites was also seen from the well-resolved lattice fringes in the high-resolution TEM image shown in Figure 1D.

On the basis of the apparent discrepancy between the XRD and Raman spectra, it seems reasonable to conclude that the rutile phase is present mainly in the inner regions of the agglomerated TiO_2 anatase nanoparticles during the anatase–rutile phase transformation. This is consistent with previous studies.[29,38–41] On the basis of TEM measurements, Penn et al.

proposed that structural elements with rutile-like character were produced at a subset of anatase interfaces, and these might serve as rutile nucleation sites.[38] Through investigation of the growth and transformation of nanometer size TiO_2 powders by in situ TEM, Lee et al. suggested that the nucleation of rutile occurred at the amorphous interface of anatase particles where there were strain and disorder.[39] On the basis of kinetic data from XRD, Zhang et al. found that rutile nucleated primarily at interfaces between contacting anatase particles when densely packed, compared to the nucleation at both interfaces and free surfaces of anatase particles with less dense packing.[40] Wang et al. suggested that rutile-like structural elements developed at the interface between anatase nanoparticles and evolved into rutile nuclei with time, followed by nuclei growth, to convert nanocrystalline anatase into rutile rapidly in the temperature range where the phase transformation does not occur in coarse anatase TiO_2.[41]

Because the rutile phase nucleates primarily at interfaces between contacting anatase nanoparticles, what else would account for this phenomenon besides the commonly suggested surface extra free energy? Is there any heat sink effect or selective heating in the anatase/rutile interface to promote the transformation of anatase into rutile after nucleation? As Raman spectroscopy is sensitive to both the anatase and rutile phases of TiO_2,[19−27] we expect it to be a suitable tool for investigating their interfaces. Different from other studies where the laser power (LP) was normally fixed, we manually changed the LP to investigate the response of the TiO_2 nanocomposites to the laser-induced heating effect.[21,22,42−45] The heating introduces changes of the Raman spectrum, from which we can deduce the temperature. Spectra were recorded after first increasing (Figure 2A and Figure S2A in the Supporting Information) and then decreasing (Figure 2B and Figure S2B in the Supporting Information) the LP (see the Supporting Information). The following peaks were observed: $E_g(a) \sim$ 146 cm^{-1}, $E_g(a) \sim$ 201 cm^{-1}, $B_{1g}(a) \sim$ 399 cm^{-1}, $A_{1g} + B_{1g}(a) \sim$ 517 cm^{-1}, and $E_g(a) \sim$ 639 cm^{-1}, for anatase;[10,20,21] $E_g(r) \sim$ 442 cm^{-1} and $A_{1g}(r) \sim$ 590 cm^{-1} for rutile.[10,19,22] The relative intensity of $E_g(a) \sim$ 201 cm^{-1} monotonously increased/decreased as the laser power increased/decreased (see Figure S2), whereas the relative intensities of $E_g(r) \sim$ 442 cm^{-1} and $A_{1g}(r) \sim$ 590 cm^{-1} decreased/increased as the LP increased/decreased. At the higher LPs, the rutile peaks became weaker or barely seen, consistent with the results of Figure 1B. For anatase, the $E_g(a)$ peak (at ~146 cm^{-1}) shifts to higher wavenumbers as LP increases, and shifts back to lower wavenumbers as LP is reduced (Figure 2C); similarly, the full width at high maximum (FWHM) increases/decreases monotonically as LP increases/decreases (Figure 2D). For rutile, instead, the $E_g(r)$ peak (~ 442 cm^{-1}) shifts to lower/higher wavenumber (Figure 2E) and the FWHM increases/decreases (Figure 2F) as LP increases/decreases.

It is well-known that laser irradiation during Raman measurements causes sample heating.[21,22,42−45] The position and width of the phonon peak can be independently used to measure the temperature.[21,22,42−45] In a previous study conducted with LP in the range 5−200 mW,[43] the position of the anatase $E_g(a)$ increased almost linearly with an increase of the local temperature, independent of the particle size, i.e., 144(150) to 145(155) cm^{-1} from 280 to 380(780) K for 17(5.5) nm nanoparticles (see the Supporting Information). To extract the peak positions in the Raman spectra of anatase TiO_2 nanoparticles in that study, we digitalized their Figure 2 and

fitted the graphs with Lorentzian functions. We then used the results of this fitting on the 17 nm nanoparticles to deduce the temperature of the anatase part in our nanocomposites. Assuming that the trend in ref 43 also holds valid in the LP range of our study, we estimate an increase of the local temperature from 300 to about 1050 K for the anatase phase, as the $E_g(a)$ shifts from 142.5 to 150.2 cm^{-1} when the LP increases from 0.76 to 478.0 mW in our work.

For bulk rutile, the $E_g(r)$ undergoes a large softening with temperature, decreasing from 448 cm^{-1} at 300 K to 405 cm^{-1} at 1150 K.[22] Although it would be obviously desirable to deduce the temperature of the rutile phase from data on nanoparticles of exactly the same size as those in the composite, to the best of our knowledge, ref 22 is the only study for rutile TiO_2 that investigates the relationship of the sample's temperature with the positions and widths of the Raman peaks. For anatase, ref 43 shows that the position of the $E_g(a)$ increases almost linearly with the increase of the local temperature, and the slope is independent of the particle size. We assumed that this property holds for the rutile phase TiO_2 as well, and used bulk rutile TiO_2's temperature-dependent Raman spectra to estimate the temperature of the 20 nm rutile phase particles in our nanocrystalline anatase−rutile composite. Because the position of the $E_g(r)$ mode of our rutile phase shifts from 445.9 to 434.5 cm^{-1} when the LP increases from 0.76 to 478.0 mW, we estimate that the temperature increases from 300 to 525 K. The reasonableness of our procedure is also supported by the fact that we observed almost identical spectra for the same commercial powder which was used in Ref 22 and for 40 nm pure commercial rutile nanoparticles we measured (see Figure S3 in the Supporting Information). We further notice that the data for anatase in ref 43. show that the change of the Raman spectrum of 17 nm relative to 10 nm particles is much smaller than that of 8 nm relative to 2 nm particles.

Altogether, the above analysis shows that the temperature in the rutile phase is much lower than that of the anatase phase under laser irradiation. To verify this conclusion, we independently estimated the local temperatures from the FWHM's temperature dependence.[22,43] For anatase, our results show that the FWHM of the $E_g(a)$ mode increases from 16.7 to 28.5 cm^{-1} when the LP increases from 0.76 to 478.0 mW. The $E_g(a)$'s FWHM increased from 8.9 to 10.2 cm^{-1} and the local temperature changed from 280 to 380 K when the LP increased from 5 to 200 mW in a previous study.[43] Assuming that the local temperature increases linearly with LP also in our case, we infer that the temperature of our anatase nanoparticles is ~1180 K when the LP is 478.0 mW. For rutile, the FWHM of the $E_g(r)$ mode was reported to increase linearly from 32 to 78 cm^{-1} when the sample's temperature increased from 300 to 1200 K.[22] In our case, the FWHM of the $E_g(r)$ mode increases from 41.5 to 56.9 cm^{-1} when the LP increases from 0.76 to 478.0 mW, suggesting a temperature change from 300 to ~601 K.

Thus, independent analysis of the Raman peak position and FWHM values provide very similar estimates of the local temperature changes for the anatase and rutile phases in the composite, notably the local temperature of the anatase phase is much higher than that of the rutile phase at higher LPs, the temperature difference between the two phases becoming larger when the LP increases. Apparently, the heat dissipation is directional, occurring preferentially towards the anatase phase. This asymmetric heating should make the phase transition from
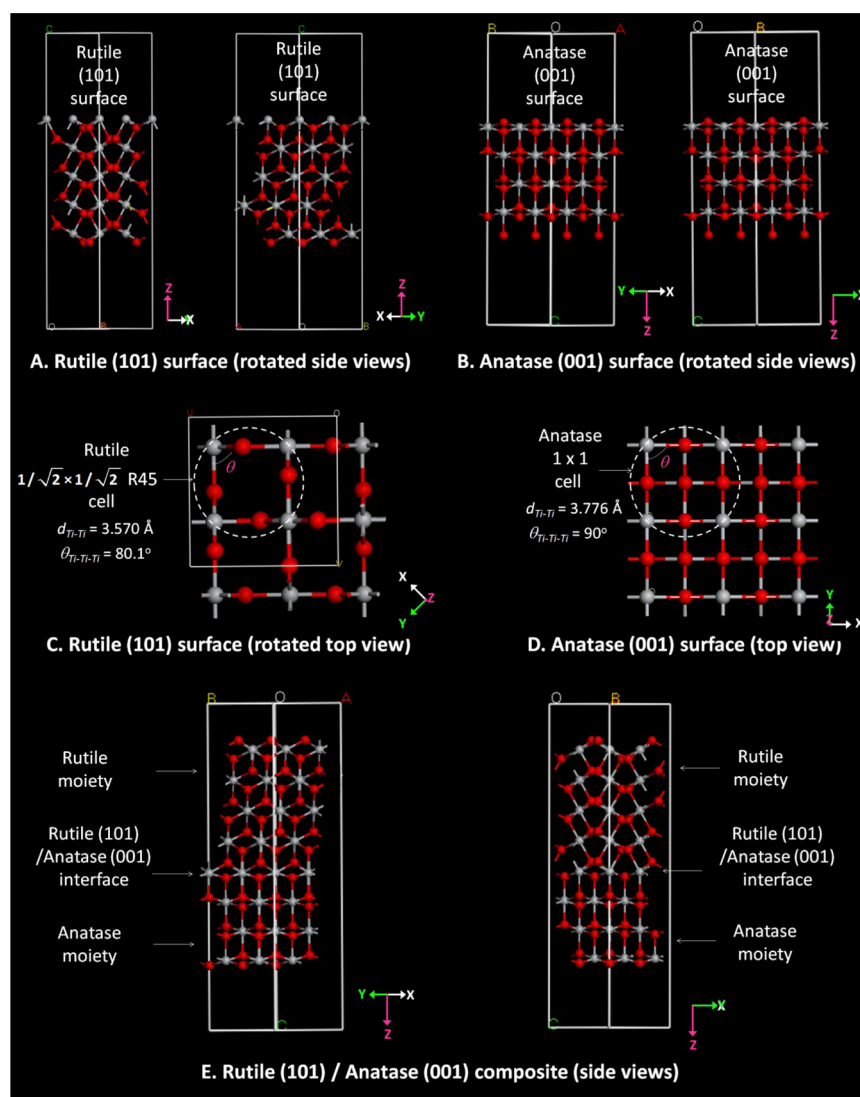
Figure 3. Illustration of model building of the rutile (101)/anatase (001) interface. (A) Crystal models of the TiO$_2$ rutile (101) surface, (B) anatase (001) surface, (C) the $1/(2)^{1/2} \times 1/(2)^{1/2}$ R45 (rotated 45°) cell in the rutile (101) surface, (D) the 1×1 cell in anatase (001) surface, and (E) rutile (101)/anatase (001) interface in the composite. The dashed lines in C and D highlight the junction cells which are merged to form the interface in the composite.

anatase to rutile much easier at the interface in the nanocomposites, as indeed observed in many studies.[38−41]

To further understand our observations, we built a theoretical lattice model of the rutile/anatase interface in the composite. Among the many possible combinations of rutile and anatase atomic surfaces, we found that rutile (101) and anatase (001) show the closest bonding arrangements and parameters. These are minority surfaces in the Wulff shapes of the corresponding crystal phases, and, having relatively high energies, they have also a stronger tendency to form interfaces than the most frequent and stable rutile (110) and anatase (101) surfaces.[35,46−49] We thus constructed a rutile/anatase interface by connecting a rutile (101) slab (Figure 3A) with an anatase (001) slab (Figure 3B). The $(1/(2)^{1/2} \times 1/(2)^{1/2})$R45 cell (R45: rotated 45°) in the rutile (101) surface (Figure 3C) has a Ti−Ti distance (d_{Ti}) of 3.57 Å, and Ti−Ti−Ti angles ($\theta_{Ti−Ti−Ti}$) of 80.1 and 99.9°. The 1×1 cell in the anatase (001) surface (Figure 3D) has a d_{Ti} of 3.78 Å and $\theta_{Ti−Ti−Ti}$ of 90°. We assumed that the structural parameters of the interface have intermediate values, specifically 3.68 Å for the Ti−Ti distance

(2.6% distortion), and 85 and 95° for the Ti−Ti−Ti bond angles (5.6% distortion) (Figure 3E). Upon relaxation of the atomic coordinates using density functional theory (DFT) calculations, only minor changes of the assumed interface structure took place.

We also studied the electronic structure of the anatase/rutile interface with DFT. Figure 4A and 4B show the computed density of states (DOSs) and projected DOSs (pDOSs), respectively, of the bulk anatase and rutile phases, the anatase (001) and rutile (101) surfaces, and the rutile (101) / anatase (001) interface. The corresponding electronic band structures are shown in Figures S4−S8 in the Supporting Information. The extent of the mixing of the O 2p orbitals and Ti 3d orbitals in the rutile (101) / anatase (001) interface is larger than that present in bulk anatase, anatase (001), rutile (101), or bulk rutile (Figure 4B). The three-dimensional (3D) and two-dimensional (2D) charge density maps of the interface (Figure 5A and Figure S9 in the Supporting Information) show indeed that at the interface the oxygen atoms have lower charge densities and the titanium atoms gain higher charge densities
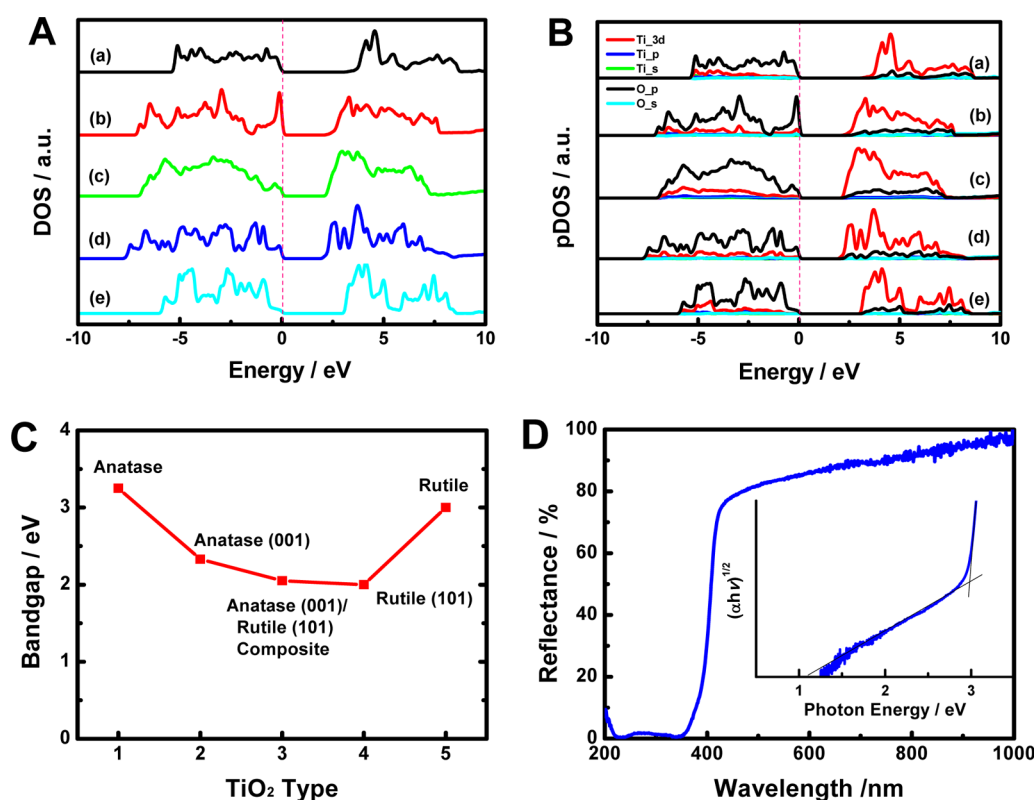
Figure 4. (A) Computed density of states (DOSs) and (B) projected density of states (pDOSs) of (a) bulk anatase, (b) anatase (001) surface, (c) anatase (001)/rutile (101) interface, (d) rutile (101) surface, and (e) bulk rutile. The vertical dotted lines indicate the Fermi levels. The corresponding electronic band structures are shown in the Supporting Information. (C) Computed bandgaps after addition of a "scissor" value of 1.25 eV, used to match the experimental band gap of bulk anatase. (D) Diffuse UV−vis reflectance spectrum of the anatase/rutile composite. The inset shows the Tauc plot.
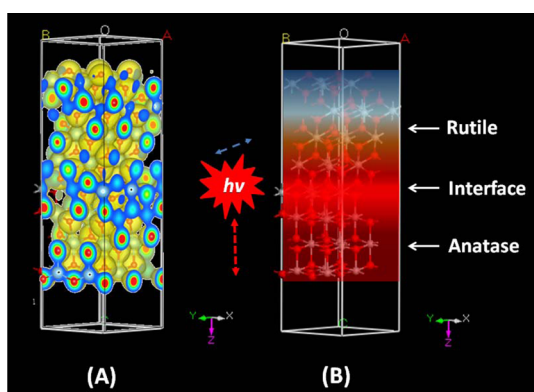
Figure 5. Charge density of the TiO_2 composite and the directional heating effect. (A) 3D charge density map of the rutile (101)/anatase (001) composite. The charge density increases as the color changes from blue to red. (B) Qualitative illustration of the directional heating effect from the rutile (101)/anatase (001) interface to the rutile and anatase phases in the composite. Red and blue represents hot and cool area, respectively.

than the corresponding atoms in the anatase or rutile moieties, confirming a stronger covalent character for the Ti−O bonds and more delocalized charge density at the interface. As DFT notoriously underestimates band gaps, the experimental band gap value of bulk anatase, 3.2 eV, was used as a reference to determine a "scissor" value of 1.25 eV, which was then applied to the band gaps of all the other systems.[10] In this way, the computed band gap of bulk rutile TiO_2 is 3.0 eV, very similar to

the experimental value, whereas the anatase (001) and rutile (101) surfaces have smaller band gaps, 2.3 and 2.0 eV, respectively (Figure 4C), due to the presence of surface states.[50,51] With the same correction, the band gap of the anatase (001)/rutile (101) interface is 2.1 eV, i.e., intermediate between those of the separate anatase (001) and rutile (101) surfaces (Figure 4C), because some of the surface states are removed in the interface.

In this experiment, the band gap can be determined by measuring the optical properties. The diffuse UV−vis reflectance spectrum (Figure 4D) of the composite shows a gradual decrease from 98% near 1000 nm to 80% near 416 nm, followed by a sharp drop to 5% near 350 nm and a small hump near 200 nm. The Tauc plot in the inset suggests a main band gap of 3.0 eV and a smaller bandgap of 1.2 eV.[16] The sharp absorption around 3 eV is due to the bulk of the rutile and anatase phases in the composite. The smaller band gap associated with the long-tail absorption and smaller than our calculated band gap for the interface can be attributed to defect states in the anatase−rutile composite,[16] not present in our ideal interface model. This result is consistent with the suggestion that the rutile phase acts as an antenna to extend the photoactivity into visible wavelengths, and catalytic "hot spots" exist at the rutile−anatase interface.[11]

On the basis of the above results, we propose to rationalize the directional heating effect across the rutile/anatase interface as follows (Figures 5B). The interface has a smaller band gap than bulk rutile and anatase, as indicated by the DFT calculations and by the experimental optical bandgap of ∼1.2 eV in the composite. Thus, it can absorb the laser excitation

9888

dx.doi.org/10.1021/am402983k | ACS Appl. Mater. Interfaces 2013, 5, 9883−9890

with wavelength of 785 nm. Part of the absorbed photon energy transfers into phonon energy, heating up the rutile–anatase interface. The lattice vibrations at the interface can propagate either along or across the interface. As suggested by our anatase–rutile interface model, the propagation across the interface is more effective in dissipating the energy, because it directly changes the Ti–O bond lengths by either dragging or pushing the adjacent Ti–O layers. Anatase [001] is a soft axis, Young's modulus along [001] being much smaller than for any other direction of anatase and rutile.[52,53] Thus phonons' amplitudes along [001] in anatase are larger than along the rutile [101] direction, causing the anatase phase to heat up more efficiently than the rutile one.

In conclusion, in this work, we have identified unique electronic and thermal characteristics of the rutile/anatase interface, notably deep tail states with absorption in the near infrared, and directional heat dissipation across the interface. This asymmetric heat dissipation at the interface can explain the facilitated phase transition from anatase to rutile at the interface in the nanocomposites after nucleation. Based on an explicit plausible model of the interface, this effect is attributed to the distinctly different elastic properties of the anatase and rutile phases at the interface. By contributing to the fundamental understanding of the differences between the TiO_2 anatase and rutile polymorphs,[54] our results can be useful for the development of TiO_2 materials with enhanced performance.

■ ASSOCIATED CONTENT

Ⓢ Supporting Information

Synthetic and analytical methods, calculation details, Figure S1–S9 and Table S1. This material is available free of charge via the Internet at http://pubs.acs.org."

■ AUTHOR INFORMATION

Corresponding Author

*E-mail: chenxiaobo@umkc.edu. Phone: +1-816-235-6420.

Author Contributions

X.C. conceived the idea. T.X. performed the sample preparation and Raman and XRD measurements, N.L. performed the theoretical calculations with suggestions by A.S. Y.Z. helped the Raman data analysis. M.B.K. helped the interpretation of Raman data. J.M. helped XRD measurements. X.C. conducted the TEM measurements. X.C. and A.S. co-wrote the paper. All authors discussed the results and commented on the manuscript. All authors have given approval to the final version of the manuscript.

Notes

The authors declare no competing financial interest.

■ ACKNOWLEDGMENTS

■ REFERENCES

(1) Fujishima, A.; Honda, K. *Nature* **1972**, *238*, 37–38.

(2) Borgarello, E.; Kiwi, J.; Pelizzetti, E.; Visca, M.; Grätzel, M. *Nature* **1981**, *289*, 158–160.

(3) Chen, X.; Li, C.; Grätzel, M.; Kostecki, R.; Mao, S. S. *Chem. Soc. Rev.* **2012**, *41*, 7909–7937.

(4) Chen, X.; Mao, S. S. *Chem. Rev.* **2007**, *107*, 2891–2959.

(5) Jun, Y. W.; Casula, M. F.; Sim, J. H.; Kim, S. Y.; Cheon, J.; Alivisatos, A. P. *J. Am. Chem. Soc.* **2003**, *125*, 15981–15985.

(6) Chen, X.; Burda, C. *J. Am. Chem. Soc.* **2008**, *130*, 5018–5019.

(7) Burda, C.; Lou, Y.; Chen, X.; Samia, A. C. S.; Stout, J.; Gole, J. L. *Nano Lett.* **2003**, *3*, 1049–1051.

(8) Choi, W.; Termin, A.; Hoffmann, M. R. *J. Phys. Chem.* **1994**, *98*, 13669–13679.

(9) Asahi, R.; Morikawa, T.; Ohwaki, T.; Aoki, K.; Taga, Y. *Science* **2001**, *293*, 269–271.

(10) Chen, X.; Liu, L.; Yu, P. Y.; Mao, S. S. *Science* **2011**, *331*, 746–750.

(11) Hurum, D. C.; Agrios, A. G.; Gray, K. A.; Rajh, T.; Thurnauer, M. C. *J. Phys. Chem. B* **2003**, *107*, 4545–4549.

(12) Ohno, T.; Tokieda, K.; Higashida, S.; Matsumura, M. *Appl. Catal. A* **2003**, *244*, 383–391.

(13) Bacsa, R. R.; Kiwi, J. *Appl. Catal. B* **1998**, *16*, 19–29.

(14) Zhang, X.; Lin, Y.; He, D.; Zhang, J.; Fan, Z.; Xie, T. *Chem. Phys. Lett.* **2011**, *504*, 71–75.

(15) Kho, Y. K.; Iwase, A.; Teoh, W. Y.; Mädler, L.; Kudo, A.; Amal, R. *J. Phys. Chem. C* **2010**, *114*, 2821–2829.

(16) Xia, T.; Otto, J. W.; Dutta, T.; Murowchick, J.; Caruso, A. N.; Peng, Z.; Chen, X. *J. Mater. Res.* **2013**, *28*, 326–332.

(17) Li, G.; Gray, K. A. *Chem. Phys.* **2007**, *339*, 173–187.

(18) Deskins, N. A.; Kerisit, S.; Rosso, K. M.; Dupuis, M. *J. Phys. Chem. C* **2007**, *111*, 9290–9298.

(19) Portq, S. P. S.; Fleury, P. A.; Damen, T. C. *Phys. Rev.* **1967**, *154*, 522–526.

(20) Ohsaka, T.; Izumi, F.; Fujiki, Y. *J. Raman Spectr.* **1978**, *7*, 321–324.

(21) Zhu, K.-R.; Zhang, M.-S.; Chen, Q.; Yin, Z. *Phys Lett. A* **2005**, *340*, 220–227.

(22) Lan, T.; Tang, X.; Fultz, B. *Phys. Rev. B* **2012**, *85*, 094305/1–094305/11.

(23) Kelly, S.; Pollak, F. H.; Tomkiewicz, M. *J. Phys. Chem. B* **1997**, *101*, 2730–2734.

(24) Bersani, D.; Lottici, P. P.; Ding, X.-Z. *Appl. Phys. Lett.* **1998**, *72*, 73–75.

(25) Ivanda, M.; Musić, S.; Gotić, M.; Turković, A.; Tonejc, A. M.; Gamulin, O. *J. Mol. Struct.* **1999**, *480-481*, 641–644.

(26) Zhang, W. F.; He, Y. L.; Zhang, M. S.; Yin, Z.; Chen, Q. *J. Phys. D: Appl. Phys.* **2000**, *33*, 912–916.

(27) Li Bassi, A.; Cattaneo, D.; Russo, V.; Bottani, C. E.; Barborini, E.; Mazza, T.; Piseri, P.; Milani, P.; Ernst, F. O.; Wegner, K.; Pratsinis, S. E. *J. Appl. Phys.* **2005**, *98*, 074305.

(28) Tian, F.; Zhang, Y.; Zhang, J.; Pan, C. *J. Phys. Chem. C* **2012**, *116*, 7515–7519.

(29) Zhang, J.; Li, M.; Feng, Z.; Chen, J.; Li, C. *J. Phys. Chem. B* **2006**, *110*, 927–935.

(30) Zhang, J.; Xu, Q.; Li, M.; Feng, Z.; Li, C. *J. Phys. Chem. C* **2009**, *113*, 1698–1704.

(31) Satoh, N.; Nakashima, T.; Yamamoto, K. *Sci. Rep.* **2013**, *3*, 1959/1–1959/6.

(32) Ricci, P. C.; Carbonaro, C. M.; Stagi, L.; Salis, M.; Casu, A.; Enzo, S.; Delogu, F. *J. Phys. Chem. C* **2013**, *117*, 7850–7857.

(33) Chatterjee, A.; Wu, S.-B.; Chou, P.-W.; Wong, M. S.; Cheng, C.-L. *J. Raman Spectrosc.* **2011**, *42*, 1075–1080.

(34) Lee, H.-Y.; Lan, W.-L.; Tseng, T. Y.; Hsu, D.; Chang, Y.-M.; Lin, J. G. *Nanotechnology* **2009**, *20*, 315702/1–315702/5.

(35) Diebold, U. *Surf. Sci. Rep.* **2003**, *48*, 53–229.

(36) He, Y.; Tilocca, A.; Dulub, O.; Selloni, A.; Diebold, U. *Nat. Mater.* **2009**, *8*, 585–589.

(37) Yang, H. G.; Sun, C. H.; Qiao, S. Z.; Zou, J.; Liu, G.; Smith, S. C.; Cheng, H. M.; Lu, G. Q. *Nature* **2008**, *453*, 638–641.

(38) Penn, R. L.; Banfield, J. F. *Am. Mineral.* **1999**, *84*, 871–876.

9889

dx.doi.org/10.1021/am402983k | *ACS Appl. Mater. Interfaces* 2013, 5, 9883–9890

(39) Lee, G. H.; Zuo, J. -M. *J. Am. Ceram. Soc.* **2004**, *87*, 473−479.

(40) Zhang, H. Z.; Banfield, J. F. *J. Mater. Res.* **2000**, *15*, 437−448.

(41) Wang, J.; Mishra, A. K.; Zhao, Q.; Huang, L. *J. Phys. D: Appl. Phys.* **2013**, *46*, 255303.

(42) Jalilian, R.; Sumanasekera, G. U.; Chandrasekharan, H.; Sunkara, M. K. *Phys. Rev. B* **2006**, *74*, 155421/1−155421/5.

(43) Sahoo, S.; Arora, A. K.; Sridharan, V. *J. Phys. Chem. C* **2009**, *113*, 16927−16933.

(44) Tang, H.; Herman, I. P. *Phys. Rev. B* **1991**, *43*, 2299−2304.

(45) Burke, H. H.; Herman, I. P. *Phys. Rev. B* **1993**, *48*, 15016−15024.

(46) Tilocca, A.; Selloni, A. *J. Chem. Phys.* **2003**, *119*, 7445.

(47) Tilocca, A.; Selloni, A. *Langmuir* **2004**, *20*, 8379−8384.

(48) Tilocca, A.; Selloni, A. *J. Phys. Chem. B* **2004**, *108*, 4743−4751.

(49) Gong, X.-Q.; Selloni, A.; Batzill, M.; Diebold, U. *Nat. Mater.* **2006**, *5*, 665−670.

(50) Tao, J.; Luttrell, T.; Batzill, M. *Nat. Chem.* **2011**, *3*, 296−300.

(51) Thomas, A. G.; Flavell, W. R.; Mallick, A. K.; Kumarasinghe, A. R.; Tsoutsou, D.; Khan, N.; Chatwin, C.; Rayner, S.; Smith, G. C.; Stockbauer, R. L.; Warren, S.; Johal, T. K.; Patel, S.; Holland, D.; Taleb, A.; Wiame, F. *Phys. Rev.* **2007**, *75*, 035105/1−035105/12.

(52) Thulin, L.; Guerra, J. *Phys. Rev. B* **2008**, *77*, 195112/1−195112/1.

(53) Yin, W.-J.; Chen, S.; Yang, J.-H.; Gong, X.-G.; Yan, Y.; Wei, S.-H. *Appl. Phys. Lett.* **2010**, *96*, 221901/1−221901/3.

(54) Xu, M.; Gao, Y.; Moreno, E. M.; Kunst, M.; Muhler, M.; Wang, Y.; Idriss, H.; Wöll, C. *Phys. Rev. Lett.* **2011**, *106*, 138302/1−138302/4.

9890

dx.doi.org/10.1021/am402983k | *ACS Appl. Mater. Interfaces* 2013, 5, 9883−9890